The regioselectivity in Diels-Alder cycloadditions of $^{\#6094}C_{68}$ fullerene with a triplet ground state

Albert Artigas,[1] Israel Fernández*,[2] and Miquel Solà*,[1]

[1] *Institut de Química Computacional i Catàlisi (IQCC) and Departament de Química, Universitat de Girona, C/ Maria Aurèlia Capmany 69, 17003 Girona, Catalonia, Spain.*
[2] *Departamento de Química Orgánica I and Centro de Innovación en Química Avanzada (ORFEO-CINQA), Facultad de Ciencias Químicas, Universidad Complutense de Madrid, 28040-Madrid, Spain.*

ABSTRACT

To achieve a full control on the regioselectivity of chemical additions to fullerenes is a major goal in the field of the reactivity of carbon nanostructures. In this work, we computationally analyze the regioselectivity of the Diels-Alder (DA) reaction of cyclopentadiene to the hollow non-isolated pentagon rule (IPR) $^{\#6094}C_{68}$ fullerene, which possesses a triplet ground state. Our aim is to check whether the typically favored [6,6]-addition in fullerenes can be shifted to [5,6] bonds in $^{\#6094}C_{68}$ due to the change in their ground states. Our results show that the [5,5] adduct is the thermodynamic reaction product whereas the kinetic product is the [5,6] bond of type F, adjacent to a pentalene unit. As compared to the singlet state, in the triplet state, the Gibbs barrier for the attack to the [5,6] bond of $^{\#6094}C_{68}$ is reduced by about 5 kcal·mol^{-1}, the DA cycloaddition becoming more regioselective. Our energy decomposition analysis shows that the change of regioselectivity in the DA reaction of hollow fullerenes from the usual [6,6] bond to the [5,6] bond in $^{\#6094}C_{68}$ is driven by higher stabilizing orbital interactions in the latter bond favored by the spin density accumulation around the two pentalene units of the cage. The findings of this investigation complement those of earlier studies on the regioselectivity of IPR fullerenes and endohedral metallofullerenes.

TOC

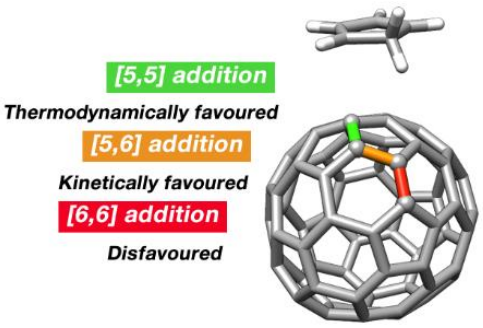

INTRODUCTION

Fullerenes are hollow cage molecules formed exclusively by carbon atoms arranged in a variable number of hexagons and twelve pentagons.[1-3] Since the discovery of C_{60},[4] many different hollow fullerenes have been reported. The great majority follows the so-called isolated pentagon rule (IPR) formulated by Kroto.[5] This rule states that fullerenes with isolated pentagons are preferred to those containing adjacent five-membered rings (5-MRs). The reason behind this preference is that bonds shared by two pentagons (pentalene units) increase the local strain affording less-stable molecules. Indeed, the pentagonal adjacency penalty rule (PAPR) quantifies the destabilization produced by adjacent pentagon pairs (APPs) in 19-24 kcal·mol^{-1} per APP.[6] Stabilization of non-IPR fullerene molecules[7] can be achieved by releasing the strain generated by fused 5-MRs through exohedral functionalization like in $C_{50}Cl_{10}$[8] or by inclusion of metal clusters in endohedral metallofullerenes (EMFs) such as $Sc_2@C_{66}$[9] or $Sc_3N@C_{68}$.[10,11] Non-IPR fullerenes are expected to be more reactive than their IPR counterparts. In 2012, the non-IPR fullerene $^{\#6094}C_{68}$ was produced and captured as a chloride $C_{68}Cl_8$.[12] $^{\#6094}C_{68}$ cannot be isolated in the bulk and, therefore, this elusive cage is just an intermediate that can be captured by chlorination. Interestingly, $^{\#6094}C_{68}$ is one of the few hollow non-functionalized fullerenes that has a triplet ground state.[13] The stability of the triplet ground state of $^{\#6094}C_{68}$ is attributed to the aromatic character of this electronic state[13] as compared to the antiaromatic character of its singlet state.[12] The singlet-triplet splitting energy in $^{\#6094}C_{68}$ was calculated to be as high as ca. 8 kcal·mol^{-1}.[13]

Fullerenes obeying the isolated pentagon rule (IPR) have two different types of C–C bonds: the [6,6] bonds in the ring junctions between two 6-MRs and the [5,6] bonds in the connection between an hexagon and a pentagon. For non-IPR species, one has also to consider the presence of [5,5] bonds (see Scheme 1 for the different bond types). The [6,6] bonds are more reactive than the [5,6] bonds in IPR hollow fullerenes, while [5,6] additions are more common in EMFs.[14,15] From a synthetic point of view, it would be desirable to have a control on the regioselectivity of the exohedral cycloadditions to fullerenes.[1,16] Several years ago, some of us found that successive reductions of C_{60} (C_{60}^{-q}, q = 0–6) modify the regioselectivity of the Diels-Alder (DA) additions, from the usual [6,6] addition in neutral species to addition to the [5,6] bond when the number of electrons added to C_{60} was higher than four.[17] This modification of the regioselectivity was explained through the local aromaticity changes in the 5- and 6-MRs of the fullerene in the reduction process. Electrons added to the cage accumulate in the 5-

MRs that gain cyclopentadienyl anion character, increasing significantly their aromaticity. In this situation, addition to a [5,6] bond of type D ($[5,6]_D$), which involves breaking the aromaticity of a unique 5-MR, becomes more favorable than addition to a [6,6] bond of type A that destroys the aromaticity of two 5-MRs. Unfortunately, an experimental proof of this change of reactivity was not possible because of the difficulties associated with generating cycloadducts from highly negatively charged fullerenes like C_{60}^{-5} or C_{60}^{-6}. More recently, some of us reported that the regioselectivity of the DA cycloaddition changes from [6,6] to [5,6] addition when the spin of the fullerenic cage is increased.[18] Indeed, for the triplet C_{60}, the most favored addition is already the [5,6] addition. Not only for the triplet, but also for high spin states, the most favored product is the [5,6] adduct, whereas in the ground state is the [6,6] product. As before, the origin of this change in the regioselectivity is connected to the local aromatic character of the molecular cage. In open-shell C_{60}, the spin density accumulates in the 5-MRs that may become more aromatic by getting more triplet cyclopentadienyl cation character. Again, addition to a $[5,6]_D$ bond, which involves breaking the aromaticity of a unique 5-MR, is favored over addition to a $[6,6]_A$ bond that cancels the aromaticity of two 5-MRs. Despite computations predict a change of regioselectivity when moving from S_0 to T_1, experimental results showed that the DA between isoindene and photoexcited $^3C_{60}$ also generates the [6,6] adduct instead of the predicted [5,6] one.[18] By analyzing the reaction in more detail, we computationally found that in the T_1 state the reaction goes through an intersystem crossing (ISC) to reach the S_0 state. When this happens, the reaction ends up in the ground state therefore affording the expected [6,6] product.

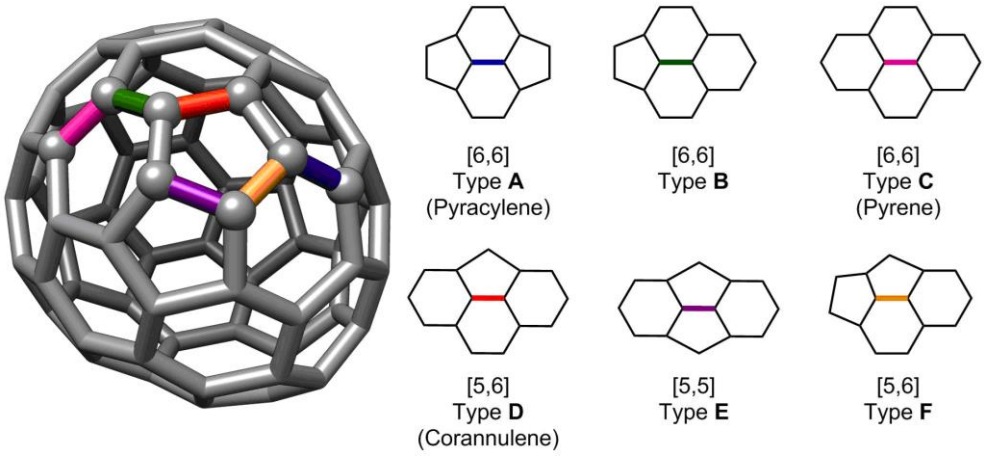

Scheme 1. Classification of the different bond types that are present in fullerene $^{\#6094}C_{68}$.

Taking into account that the triplet C_{60} yields the [6,6] product due to the occurrence of an ISC and that such ISC is not expected to occur in $^{\#6094}C_{68}$ because this system has already a T_0 ground state, we thought that $^{\#6094}C_{68}$ could be one of the few hollow non-functionalized fullerenic cages that prefers the [5,6] over the [6,6] addition in DA reactions. To check this hypothesis, we have computationally studied all possible additions to $^{\#6094}C_{68}$ (see Figure 1 for all different bonds of $^{\#6094}C_{68}$). For the most stable products, we have also located the transition states. We anticipate here that our results show that, for $^{\#6094}C_{68}$, the most reactive [5,6] bond reacts much faster than the most reactive [6,6] bond. It is worth noting that the DA cycloaddition to C_{68} has been studied before.[19] However, the cage considered was the $^{\#6140}C_{68}$ that has a singlet ground state. For this non-IPR fullerene, the [5,5] bond was reported to be the most favored thermodynamically, whereas kinetically the most reactive bond was a [5,6] bond of F type next to the pentalene unit.[19]

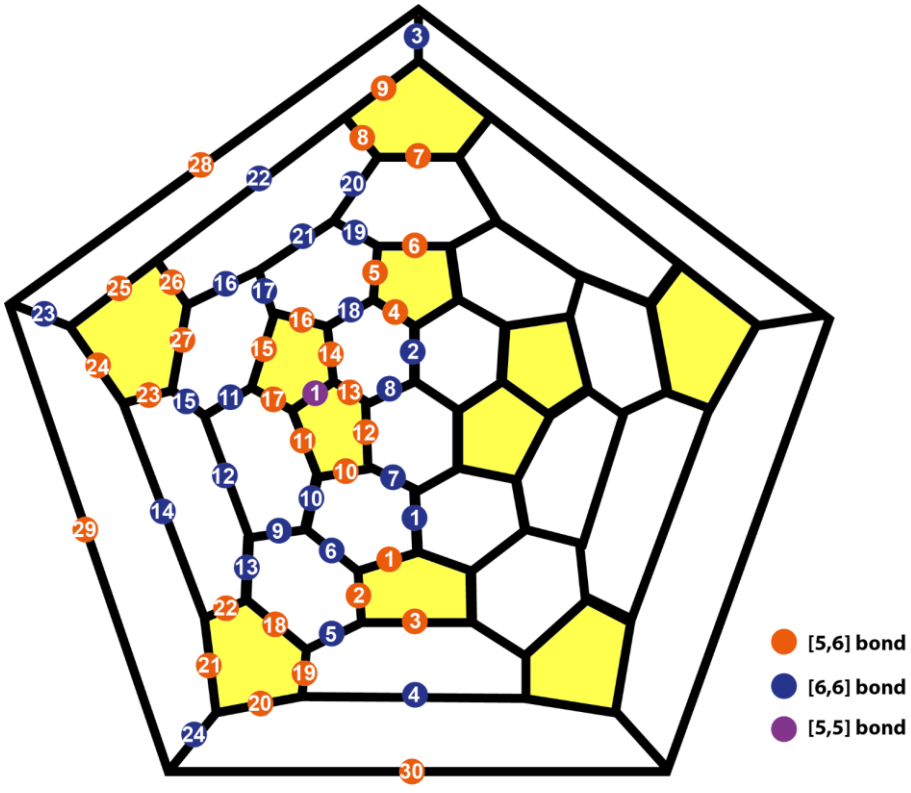

Figure 1. Schlegel diagram of $^{\#6094}C_{68}$ with labels considered in this work for all different bonds.

COMPUTATIONAL DETAILS

All geometry optimizations were performed with the Gaussian 16 package[20] by using the UB3LYP hybrid density functional[21,22] with the D3 Grimme's corrections for dispersion[23] and the 6-31G(d,p) basis set[24] without symmetry constraints. Analytical Hessians were computed to confirm that the optimized structures are indeed minima (zero imaginary frequencies) or transition states (one imaginary frequency). $<S^2>$ values computed at the UB3LYP/6-31G(d,p) values were analyzed for all stationary points of the [5,5], $[5,6]_D$, $[5,6]_F$ and [6,6] studied reaction paths to assess the extent of spin contamination (See Table S2 in the Supporting Information). For the triplet state species, only two $<S^2>$ values, corresponding to the biradical intermediate and the transition state (TS) of the first step in the [6,6] path, were found to have a $<S^2>$ value that is higher by a little bit more than 10% of the expected $<S^2> = 2$. To analyze the effect of the basis set on the optimized geometries, intermediates and TS for [5,5] and $[5,6]_F$ paths were re-optimized with the 6-311G(d,p) basis set. Superimposed geometries and RMSD values (Å) are reported in Figure S9 in the Supporting Information. No significant changes were found in any of the re-computed geometries.

The attacks to the most reactive [5,5], [5,6], and [6,6] bonds were discussed by means of the activation strain model (ASM)[25-29] of reactivity at the UM06-2X-D3/def2-TZVPP[30]//UB3LYP-D3/6-31G(d,p) level of theory. In the ASM, the bonding energy is made up of two major components (eq. 1):

$$\Delta E(\zeta) = \Delta E_{strain}(\zeta) + \Delta E_{int}(\zeta) \qquad (1)$$

In this formula, ζ is the intrinsic reaction coordinate. The strain energy (also known as distortion energy), $\Delta E_{strain}(\zeta)$, is the amount of energy required to deform the separated fragments from their equilibrium structure to the geometry that they have at position ζ of the reaction coordinate. The interaction energy $\Delta E_{int}(\zeta)$ corresponds to the actual energy change when the prepared fragments are combined to form the overall molecule at position ζ of the reaction coordinate.

The $\Delta E_{int}(\zeta)$ term can be further decomposed in the framework of the Kohn-Sham molecular orbital model by using the so-called energy decomposition analysis (EDA) method.[31-34] Within this methodology, the interaction energy is decomposed into the following chemically meaningful contributions (eq. 2):

$$\Delta E_{int}(\zeta) = \Delta E_{elstat}(\zeta) + \Delta E_{Pauli}(\zeta) + \Delta E_{orb}(\zeta) + \Delta E_{disp}(\zeta) \qquad (2)$$

The term $\Delta E_{elstat}(\zeta)$ corresponds to the classical electrostatic interaction between the unperturbed charge distributions of the prepared (*i.e.* distorted) fragments and is usually

attractive. The Pauli repulsion $\Delta E_{\text{Pauli}}(\zeta)$ comprises the destabilizing interactions between occupied molecular orbitals and it is responsible for the steric repulsion. The orbital interaction $\Delta E_{\text{orb}}(\zeta)$ accounts for bond pair formation, charge transfer, and polarization, whereas the $\Delta E_{\text{disp}}(\zeta)$ term takes into account the interactions that are due to dispersion forces. Finally, the origins of the orbital interactions were analyzed quantitatively by using the NOCV (Natural Orbital for Chemical Valence) extension of the EDA method.[35] All the EDA-NOCV calculations were performed with the ADF program[36] at the UM06-2X-D3/TZ2P level using the optimized UB3LYP-D3/6-31G(d,p) geometries. Therefore, this level is denoted UM06-2X-D3/TZ2P//UB3LYP-D3/6-31G(d,p) level of theory. In EDA, open-shell fragments were treated with spin-unrestricted formalism but, for technical reasons, spin-polarization was not included. This error causes the studied bond to become in the order of a few kcal mol^{-1} too strong, without affecting trends. DLPNO-CCSD/def2-TZVP//UB3LYP/6-31G(d,p) single-point energy calculations[37] with the def2-TZVP/C auxiliary basis set and the RIJCOSX approximation for the HF step using the def2-TZVP/J auxiliary basis set were performed with the ORCA 4.0.0.2 program.[38] The energy barriers obtained at this level of theory show the same reactivity trends as obtained at the UB3LYP-D3 and UM06-2X-D3 levels of theory and confirm the reliability of the results found with these two latter functionals. For instance, the difference in energy barriers for the [5,5]/[5,6] and [6,6] first attack (*vide infra*) are $\Delta\Delta E^{\ddagger}_{\text{DPLNO-CC}}$ = 6.1 kcal/mol, $\Delta\Delta E^{\ddagger}_{\text{UM06-2X-D3}}$ = 9.4 kcal/mol, and $\Delta\Delta E^{\ddagger}_{\text{UB3LYP-D3}}$ = 12.6 kcal/mol in favor of the [5,5]/[5,6] path. T_1 diagnostic[39] values obtained from DLPNO-CC calculations were in all cases smaller than 0.02, indicating the single reference character of the species studied.

RESULTS AND DISCUSSION

In this section, we discuss first the thermodynamics of the DA cycloadditions of cyclopentadiene (Cp) on all different bonds of $^{\#6094}C_{68}$, second, we study the kinetics of the most exothermic additions and, finally, we provide a rationale for the energy barriers of the most kinetically favored attacks with the activation strain model of reactivity combined with the EDA-NOCV method.

i. Thermodynamics of the Diels-Alder cycloadditions.

The reaction energies obtained at the UB3LYP-D3/6-31G(d,p) level for the DA addition of the cyclopentadiene over all 55 non-equivalent bonds of $^{\#6094}C_{68}$ (see Figure 1) are listed in Table 1. It is important to remark that the reaction energies presented in Table 1 are

relative energies with respect to Cp and $^{\#6094}C_{68}$ when they are infinitely separated. Table 1 also contains the spin state of the final product. In most of the additions, the most stable product has a triplet ground state. However, in some particular cases, the final most stable product has a singlet ground state instead. For all unsymmetrical isomers, both the *endo* and *exo* approaches were considered. Table 1 contains the reaction energy of the most favored approach, whereas Table S1 lists the reaction energy of all possible attacks.

Table 1. The predicted reaction energies (ΔE_R, kcal·mol^{-1}, UB3LYP-D3/6-31G(d,p) level) for the Diels-Alder reaction of cyclopentadiene over all non-equivalent bonds of $^{\#6094}C_{68}$.

[6,6] ISOMERS				**[5,6] ISOMERS**			
Bond[a]	**Spin**	**Bond type[b]**	**ΔE_R (kcal·mol^{-1})**	**Bond[a]**	**Spin**	**Bond type[b]**	**ΔE_R (kcal·mol^{-1})**
				1	0	D	-13.5
1	1	B	-0.3	**2**	1	D	-4.3
2	1	B	-12.9	**3**	0	D	5.5
3	1	A	-19.8	**4**	0	D	-16.5
4	1	A	-19.2	**5**	0	D	-1.5
5	1	A	-15.4	**6**	1	D	-4.9
6	1	B	-6.6	**7**	1	D	-3.7
7	1	B	-4.0	**8**	0	D	-2.9
8	1	B	0.0	**9**	0	D	-0.7
9	1	C	11.4	**10**	0	D	-16.8
10	0	B	-1.7	**11**	0	F	-23.3
11	1	B	4.9	**12**	1	D	-15.3
12	0	C	13.3	**13**	0	F	-31.2
13	1	B	-7.9	**14**	0	F	-20.9
14	1	A	-11.2	**15**	1	D	-9.8
15	1	B	0.2	**16**	0	D	-6.6
16	1	B	-1.2	**17**	0	F	-21.6
17	1	B	-4.9	**18**	1	D	0.1
18	1	A	-11.0	**19**	1	D	6.3
19	1	B	2.2	**20**	1	D	3.8
20	1	B	0.6	**21**	1	D	6.1

21	1	C	22.9	**22**	1	D	0.9
22	1	A	-12.8	**23**	1	D	2.0
23	1	A	-16.0	**24**	1	D	7.1
24	1	A	-14.5	**25**	1	D	2.4
				26	0	D	-3.6
[5,5] ISOMERS				**27**	1	D	-6.2
				28	1	D	2.4
Bond[a]	**Spin**	**Bond type[b]**	**ΔE_R (kcal·mol^{-1})**	**29**	1	D	4.8
1	0	E	-38.5	**30**	1	D	3.2

[a] For bond numbering, see Figure 1. [b] For bond types, see Scheme 1.

As can be seen, in general, the studied DA cycloaddition is not a very exothermic reaction. In fact, 20 attacks out of 55 are endothermic. The less reactive bonds are those in the ring junctions involving three or four 6-MRS (bond types B, C, and D), which contain the less pyramidalized C atoms. On the other hand, all additions to $[6,6]_A$ and $[5,6]_F$ bonds are exothermic. In general, cycloadditions at [5,6] bonds are somewhat more exothermic than [6,6] ones with average exothermicities of -5.3 and -4.3 kcal·mol^{-1}, respectively. The most favored thermodynamic product is that obtained from the addition attack on [5,5] bond **1** (ΔE_R = -38.5 kcal·mol^{-1}) followed by the $[5,6]_F$ bond **13** of F type (ΔE_R = -31.2 kcal·mol^{-1}). The most exothermic attack to a $[6,6]_A$ bond corresponds to type A bond **3** (ΔE_R = -19.8 kcal·mol^{-1}). Finally, bond **4** is the most thermodynamically favored addition to bonds of D type. The Bell-Evans-Polanyi plots of several Diels-Alder cycloadditions to fullerenes, EMFs, and polycyclic aromatic hydrocarbons show a good linear relationship between reaction energies and energy barriers.[40-44] For this reason, we analyzed the complete reaction pathway only for the most exothermic attacks of cyclopentadiene over $^{\#6094}C_{68}$, i.e., additions to the $[5,5]_E$ bond, $[5,6]_F$ bond **13** adjacent to a pentalene unit, $[6,6]_A$ bond **3**, and $[5,6]_D$ bond **4**. The results are discussed in the next subsection.

ii. Kinetic behavior of the Diels-Alder cycloadditions.

Scheme **2** presents a general overview of the reaction mechanism and Table **2** summarizes the reaction energies (ΔG_R, kcal·mol^{-1}) and energy barriers ($\Delta G^{\ddagger}$, kcal·mol^{-1}) for the most reactive bond of each type. As shown in Scheme 2, Diels-Alder (DA) cycloadditions to these systems occur stepwise because of the triplet ground state $^{\#6094}C_{68}$, which sharply

contrasts with most DA cycloadditions to fullerenes and endohedral metallofullerenes that proceed in a concerted manner.[15,45,46]

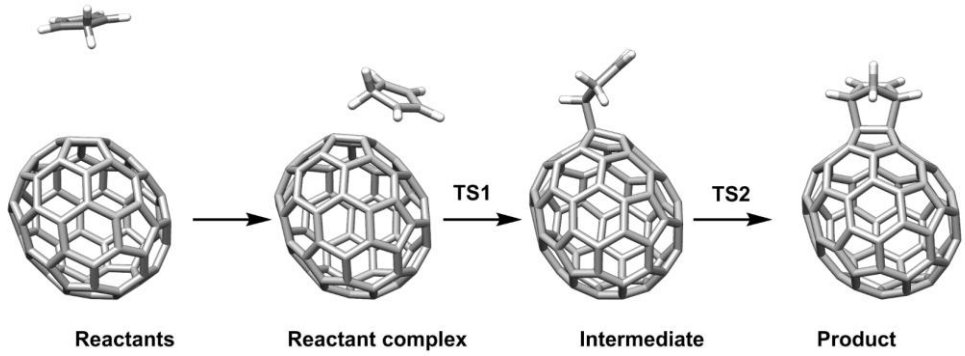

Scheme 2. General mechanism of the Diels-Alder cycloaddition involving $^{\#6094}C_{68}$ and cyclopentadiene.

Table 2. Reaction energies (ΔG_R, kcal·mol^{-1}) and energy barriers ($\Delta G^{\ddagger}$, kcal·mol^{-1}) for the Diels-Alder reaction of cyclopentadiene over the most reactive bonds of $^{\#6094}C_{68}$ in its triplet ground state. $\Delta G^{\ddagger}_{concerted}$ refers to the barriers of the Diels-Alder cycloaddition of cyclopentadiene to $^{\#6094}C_{68}$ in its singlet closed-shell state.

Cycloaddition	**ΔG_R**	**$\Delta G^{\ddagger}$**	**$\Delta G^{\ddagger}_{concerted}$**
[5,5]	-18.6	11.3	18.2
$[6,6]_A$	-2.0	25.0	27.0
$[5,6]_D$	-1.1	17.2	20.4
$[5,6]_F$	-12.6	11.3	16.1

The reaction path leading to the $[6,6]_A$ adduct **3** (see Figure S1 in the Supporting Information) takes place entirely in the triplet ground state. It is slightly exoergonic by 2 kcal·mol^{-1} and has an energy barrier of 25 kcal·mol^{-1} (Table 2). Overall, the $[6,6]_A$ adduct is the least favored among the most reactive bonds studied, both kinetically and thermodynamically. The reaction paths leading to the $[5,6]_F$ and [5,5] products are identical until the first addition takes place (Figure 2). For these $[5,6]_F$ and [5,5] reaction paths, the initial attack of the cyclopentadiene moiety takes place on C44 of $^{\#6094}C_{68}$ (see Scheme S1 in the Supporting Information and Figure 3 for atom labels) leading to the formation of a diradical intermediate. This process is exergonic by 0.5 kcal·mol^{-1} and has a Gibbs energy barrier of 11.3 kcal·mol^{-1}. It is worth mentioning that, in the regioselective chlorination of $^{\#6094}C_{68}$, the first addition of Cl to $^{\#6094}C_{68}$ also occurs at the same C44.[13] The intermediate formed in this

first step, which has a triplet ground state, evolves to the final $[5,6]_F$ and [5,5] products via a second addition that takes place through an ISC. Such ISC is expected to be very efficient given that it is known that $^1C_{60}$ can undergo ICS to $^3C_{60}$ with very high quantum yields.[47] For the [5,5] bond, the second addition is exergonic by 18.1 kcal·mol^{-1} and has an energy barrier of 5.9 kcal·mol^{-1} (see Figure S3). It is worth mentioning here that the resulting [5,5] adduct has a singlet ground state. For the $[5,6]_F$ path, the second addition is an almost barrierless process (to reach the ISC from the triplet intermediate has a cost of less than 1 kcal·mol^{-1}, see Figure S2 in the Supporting Information), and is exergonic by 12.1 kcal·mol^{-1}. Before reaching the final adduct, there is another ISC from the singlet to the triplet state, so the final regioisomer has a triplet state with a very low singlet-triplet energy gap of only 0.8 kcal·mol^{-1}. From our computational results, we conclude that the [5,5] adduct is the thermodynamic reaction product while the kinetic product is the $[5,6]_F$ one. Anyhow, our calculations firmly confirm our initial hypothesis, i.e. $^{\#6094}C_{68}$ is one of the few hollow non-functionalized fullerenic cages that prefers the [5,6] over the [6,6] addition in DA reactions. We have also analyzed the cycloaddition reaction on the most favored $[5,6]_D$ bond (Table 1). This latter bond appears to be more reactive than the $[6,6]_A$ analyzed but still much less than its [5,5] and $[5,6]_F$ counterparts. Furthermore, the geometries of the transition states (TSs) for the initial attack, which is the rate determining step of the entire process, are shown in Figure 3. As can be seen, the C–C bond length of the bond being formed ranges from 1.95 to 2.16 Å, with the more exergonic attacks having earlier TSs. Finally, we evaluated the effect of temperature on the regioselectivity by re-computing the Gibbs energy profile of [5,5] and $[5,6]_F$ paths at 373 K (See Figure S8 in the Supporting Information). No significant changes were observed with the increase in the temperature.

Such a difference in reactivity between [5,5] and $[5,6]_F$ bonds (attack to C44 carbon) on one side and $[5,6]_D$ bond (attack to C47 carbon) on the other may be attributed in part to the higher degree of pyramidalization of the [5,5] and $[5,6]_F$, the latter being clearly influenced by the adjacency to a pentalene unit (See Scheme 1). Indeed, the pyramidalization angles[48,49] of C44, C47, and C61 are 16.1º, 11.9º, and 11.9º, respectively. However, it is also important to look at the excess of α spin density (Figure 4) showing C44 with larger lobes of spin density than C61 and C47 involved in the $[6,6]_A$ and $[5,6]_D$ attacks, respectively. We have also analyzed the Diels-Alder cycloaddition of cyclopentadiene to $^{\#6094}C_{68}$ in its singlet closed-shell state to analyze the effect of changing from the triplet to the singlet state on the reactivity. As can be seen in Table 2, the Gibbs energy barriers for the singlet closed-shell state are 2 to 7 kcal·mol^{-1} higher than those of the stepwise reaction mechanism, but the regioselectivity

remains more or less the same. The most affected attacks are the [5,5] and $[5,6]_F$ with Gibbs energy barriers reduced by 7 and 5 kcal·mol^{-1}, respectively. Therefore, the triplet state favors particularly the reactivity of these two bonds and does almost not modify the reactivity of the $[6,6]_A$ bond. The higher degree of pyramidalization of the [5,5] and $[5,6]_F$ bonds explains better the higher reactivity of these bonds. The effect of the open-shell electronic structure is therefore important but not decisive. This result is in line with the fact that for the singlet $^{\#6140}C_{68}$, the [5,5] bond was reported to be the most favored thermodynamically, whereas kinetically the most reactive bond was a $[5,6]_F$ adjacent to the pentalene unit.[19]

Figure 2. UB3LYP-D3/6-31G(d,p) Gibbs energy profile for [5,5] and $[5,6]_F$ paths. Electronic relative energies are given within parenthesis. All energies are relative energies to infinitely separated reactants and are given in kcal·mol^{-1}. Blue color refers to triplet state structures.

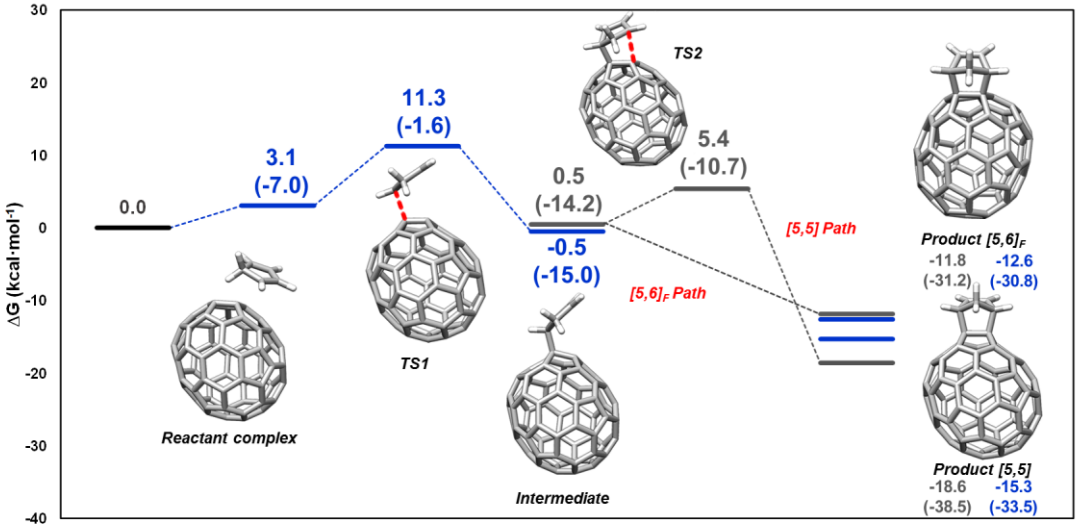

Figure 3. The optimized geometries of the transition state for the initial attack of cyclopentadiene to the most reactive a) $[6,6]_A$ bond b) $[5,6]_F$ and $[5,6]_D$ bond, and c) [5,5] bond. Distances are given in Angstroms (Å).

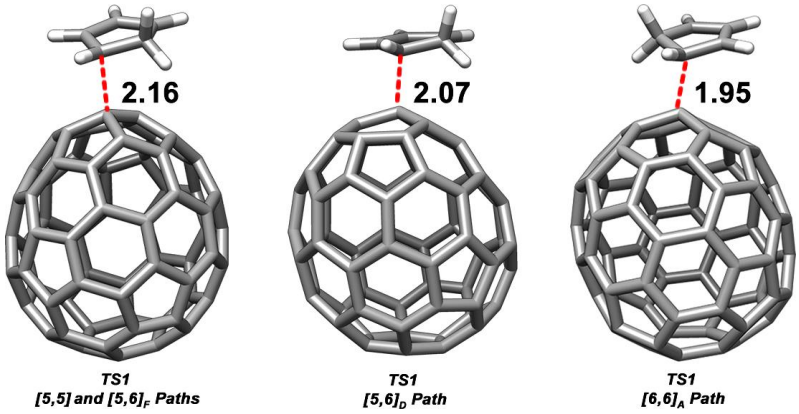

Figure 4. The excess of spin density in $^{\#6094}C_{68}$. Isosurface value of 0.004 au. By convention excess α spin density in blue is termed positive. C44, C47, and C61 indicated with an arrow.

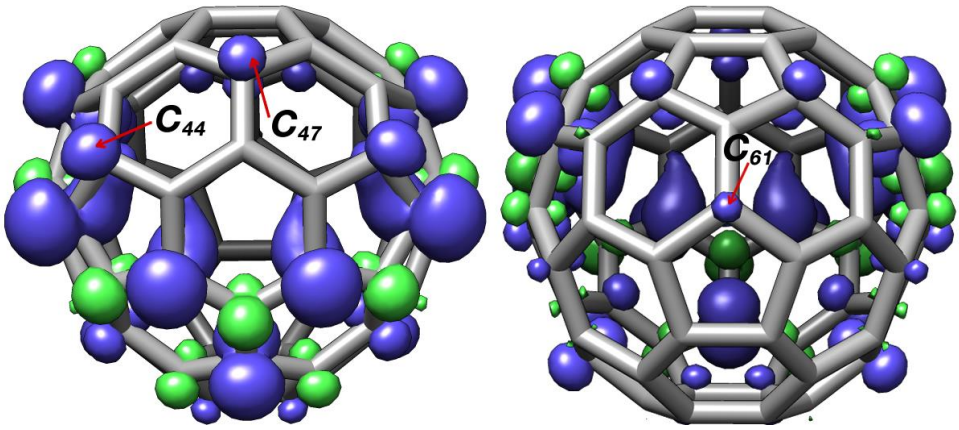

iii. Understanding the different reactivity trends.

In this last subsection, we applied the Activation Strain Model (ASM) of reactivity to quantitatively understand the origin of the different reactivity of the [5,5], $[5,6]_F$, and $[6,6]_A$ most reactive bonds of $^{\#6094}C_{68}$. We applied the ASM to the initial attack, which is the rate determining step, from the reactant complex to TS1 (see Scheme 2). [5,5] and $[5,6]_F$ cycloadditions share the same initial attack. Figure 5 shows the computed Activation Strain Diagrams (ASDs) for the [5,5]/$[5,6]_F$ and $[6,6]_A$ cycloadditions from the reactant complex up to the respective TS1s along the intrinsic reaction coordinate projected onto the forming C···C bond distance. As can be seen, for the $[6,6]_A$ cycloaddition, the strain energy is significantly less destabilizing than in the [5,5]/$[5,6]_F$ attacks from the beginning of the process up to the corresponding transition state region. Therefore, the ΔE_{strain} is not at all responsible for the higher barrier computed for the $[6,6]_A$-pathway. At variance, the interaction energy is clearly much stronger for the addition on the [5,5]/$[5,6]_F$ attacks than on the [6,6]-bond along the entire reaction coordinate. This highly stabilizing interaction between the reactants is able to offset the higher destabilizing effect of the ΔE_{strain}, which is then translated into the computed lower barrier for the process involving the [5,5]/$[5,6]_F$ bonds.

Figure 5. Comparative activation-strain diagrams of the Diels-Alder cycloaddition reactions between cyclopentadiene and the [5,5]/[5,6]$_F$ (solid lines) and [6,6]$_A$ (dashed lines) bonds of $^{\#6094}C_{68}$ along the intrinsic reaction coordinate projected onto the forming C···C bond distance. All data were computed at the UM06-2X-D3/def2-TZVPP//UB3LYP-D3/6-31G(d,p).

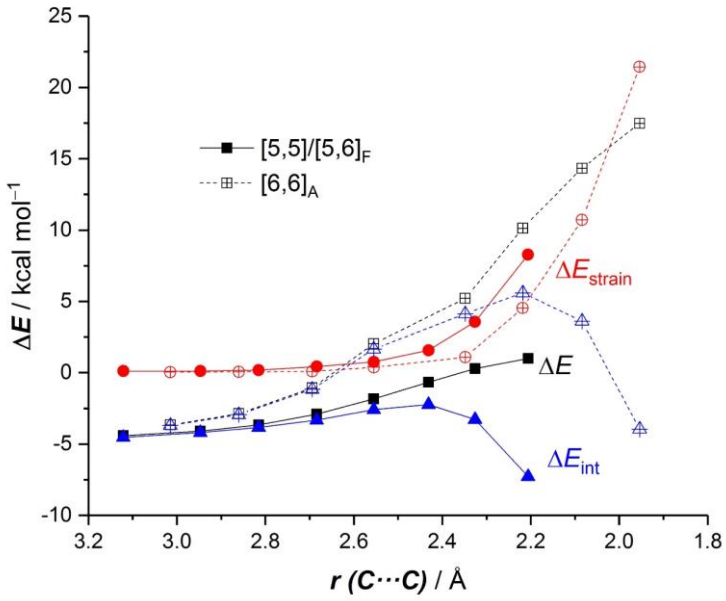

Further quantitative insight into the factors making the interaction between reactants weaker for the [6,6]$_A$ cycloaddition can be achieved by means of the EDA method. Figure 6 shows the evolution of the different contributions to the total interaction energy along the reaction coordinate for the [5,5]/[5,6]$_F$ and [6,6]$_A$ cycloadditions. The $\Delta E_{elstat}(\zeta)$ and $\Delta E_{disp}(\zeta)$ terms are almost identical for the two attacks and therefore are not decisive for the higher interaction computed for the process involving the [5,5]/[5,6]$_F$ bonds. In contrast, the [5,5]/[5,6]$_F$ addition clearly benefits from much stronger orbital interactions (ΔE_{orb}) and also, from a less destabilizing Pauli repulsion (albeit to a less extent). For instance, at the same C···C forming bond length of 2.2 Å, and for the [5,5]/[5,6]$_F$ and [6,6]$_A$, respectively, the computed ΔE_{elstat} is -32.4 and -34.4 kcal·mol^{-1}, ΔE_{Pauli} 57.6 and 63.9 kcal·mol^{-1}, ΔE_{disp} -5.7 and -6.0 kcal·mol^{-1}, whereas ΔE_{orb} is -38.8 and -29.3 kcal·mol^{-1}. The higher Pauli repulsion for the [6,6] attack can be attributed to the close proximity of the CH_2 group of the cyclopentadiene to the C_{68} cage in the TS (2.716 Å for [6,6] TS1 and 2.777 Å for [5,6] TS1). Therefore, it can be concluded that the stronger orbital interactions between the deformed reactants of the [5,5]/[5,6]$_F$ cycloaddition mainly constitute the origin of the lower barrier computed for this attack.

Figure 6. Comparative energy decomposition analysis of the Diels-Alder cycloaddition reactions between cyclopentadiene and the $[5,5]/[5,6]_F$ (solid line) and $[6,6]_A$ (dashed line) bonds of $^{\#6094}C_{68}$ along the intrinsic reaction coordinate projected onto the forming C···C bond distance. All data were computed at the UM06-2X/TZ2P//UB3LYP-D3/6-31G(d,p).

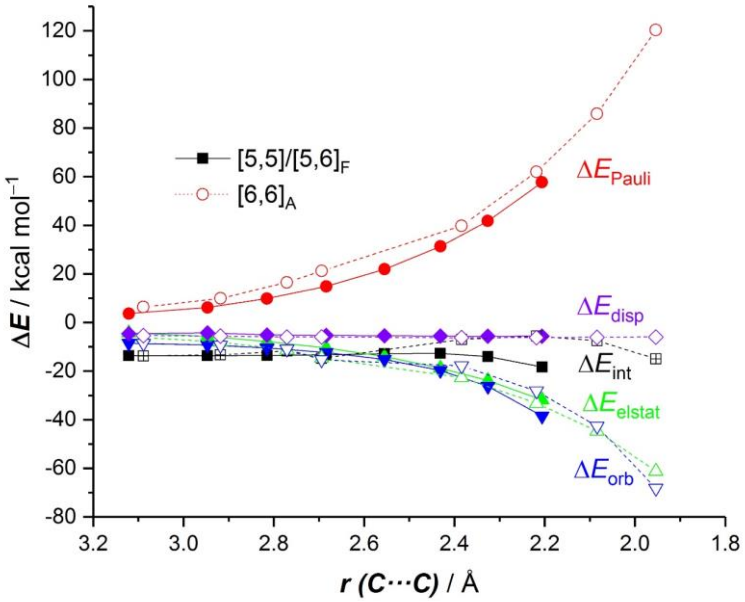

Finally, the ΔE_{orb} term has been further partitioned by using the EDA-NOCV procedure. This approach suggests that the main orbital interaction corresponds to the π(diene) → π_{SOMO}(fullerene) (see Figure 7, charge flow is red → blue) that leads to the formation of a new C–C bond and the accumulation of excess density in the cyclopentadiene. Interestingly, this dominant orbital interaction is much stronger for the $[5,5]/[5,6]_F$ attack than for the $[6,6]_A$ one, as clearly viewed from the associated stabilizing deformation energies ($\Delta E(\rho_1)$) computed at the same consistent C···C bond forming distance of 2.2. Å (see Figure 7). We attribute the observed difference to the large contribution of C44 to the SOMO of $^{\#6094}C_{68}$ and to the larger spin density in this C atom (see above), which is translated into the significantly higher $<\pi$(diene)–π_{SOMO}(fullerene)$>$ molecular orbital overlap computed for the process involving the $[5,5]/[5,6]_F$ bond (S = 0.081 vs 0.030). As a consequence of this stronger orbital interaction, the total interaction energy between the deformed reactants is also stronger for the $[5,5]/[5,6]_F$ approach, which ultimately results into the predicted [5,6]-regioselectivity.

Figure 7. Plot of the deformation densities (Δρ) of the pairwise orbital interactions between cyclopentadiene and the [5,5]/[5,6]$_F$ and [6,6]$_A$ bonds of $^{\#6094}C_{68}$ and associated stabilization energies ($\Delta E(\rho_1)$, in kcal·mol^{-1}). The color code of the charge flow is red → blue. All data computed at the UM06-2X-D3/TZ2P//UB3LYP-D3/6-31G(d,p).

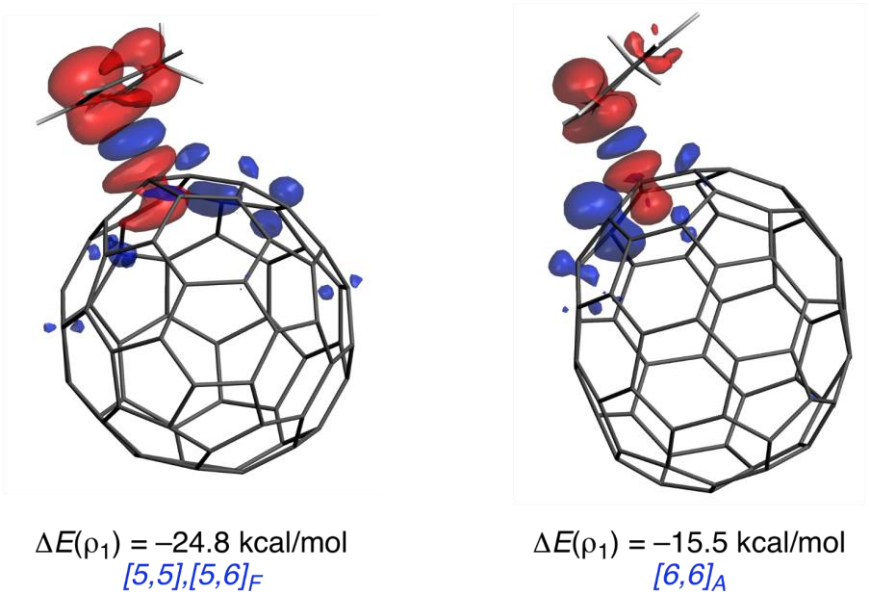

CONCLUSIONS

We have studied the regioselectivity of the Diels-Alder cycloaddition of cyclopentadiene to $^{\#6094}C_{68}$ in its triplet ground state. We have shown that $^{\#6094}C_{68}$ is one of the first reported hollow non-functionalized fullerene that favors the cycloaddition to a [5,6] instead of the typically preferred [6,6] bond. Our results indicate that the [5,5] adduct is the thermodynamic reaction product whereas the kinetic product is the [5,6]$_F$ one. This change of regioselectivity in the DA reaction of hollow fullerenes from the usual [6,6] bond to the [5,6] bond in $^{\#6094}C_{68}$ is driven by the more stabilizing orbital interaction favored by the spin density accumulation around the pentalene region of the cage.

Our results highlight important differences in the regioselectivity of Diels-Alder cycloaddition of IPR and non-IPR fullerenes. For IPR fullerenes, the [6,6] addition is preferred in the singlet closed-shell state,[45] whereas in the triplet state the preferred attack takes place on the [5,6] bond.[18] For non-IPR fullerenes, the [5,5] adduct is the thermodynamic reaction product and the [5,6]$_F$ adduct is the one obtained under kinetic control, irrespective of the

electronic state being a singlet[19] or a triplet. However, we have found that in the triplet state the regioselectivity in favor of the [5,5] and $[5,6]_F$ attacks is enhanced by 5 to 7 kcal·mol^{-1}. The findings of this research provide additional insights into the problem of the regioselectivity in fullerenes and endohedral metallofullerenes, which, in our opinion, may be useful for the experimental generation of unusual fullerene derivatives.

ACKNOWLEDGEMENTS

Financial support was provided by the Spanish Ministerio de Economía y Competitividad (MINECO) and FEDER (Grants CTQ2016-78205-P and CTQ2016-81797-REDC to I. F. and CTQ2017-85341-P to M. S.), and Catalan DIUE (projects 2017SGR39, ICREA Academia 2014 prize, and XRQTC to M. S.). The FEDER grant UNGI10-4E-801 has also funded this research. A. A. acknowledges the MINECO for a FPI grant.

SUPPORTING INFORMATION AVAILABLE

Schlegel diagram with labelling of the atoms, reaction energies for all possible attacks, Gibbs energy profiles for attacks to bonds 1, 3, 4, and 13, and linear transits from the diradical intermediate to the reaction product for the studied [5,5], $[5,6]_D$, and $[5,6]_F$ attacks. Cartesian xyz coordinates for all optimized reactants, intermediates, transition states, and products.

REFERENCES

(1) Hirsch, A.; Brettreich, M. *Fullerenes: Chemistry and Reactions*; John Wiley & Sons: Weinheim, 2004.

(2) Fowler, P. W.; Manolopoulos, D. E. *An Atlas of Fullerenes*; Clarendon Press: Oxford, 1995.

(3) *Chemistry of Nanocarbons*; John Wiley & Sons: Chichester, 2010.

(4) Kroto, H. W.; Heath, J. R.; O'Brien, S. C.; Curl, R. F.; Smalley, R. E. C_{60} - Buckminsterfullerene. *Nature* **1985**, *318*, 162-163.

(5) Kroto, H. W. The stability of the fullerenes C_n, with n = 24, 28, 32, 36, 50, 60 and 70. *Nature* **1987**, *329*, 529 - 531.

(6) Albertazzi, E.; Domene, C.; W. Fowler, P.; Heine, T.; Seifert, G.; Van Alsenoy, C.; Zerbetto, F. Pentagon adjacency as a determinant of fullerene stability. *Phys. Chem. Chem. Phys.* **1999**, *1*, 2913-2918.

(7) Tan, Y.-Z.; Xie, S.-Y.; Huang, R.-B.; Zheng, L.-S. The stabilization of fused-pentagon fullerene molecules. *Nature Chem.* **2009**, *1*, 450.

(8) Xie, S.-Y.; Gao, F.; Lu, X.; Huang, R.-B.; Wang, C.-R.; Zhang, X.; Liu, M.-L.; Deng, S.-L.; Zheng, L.-S. Capturing the Labile Fullerene[50] as $C_{50}Cl_{10}$. *Science* **2004**, *304*, 699-699.

(9) Wang, C.-R.; Kai, T.; Tomiyama, T.; Yoshida, T.; Kobayashi, Y.; Nishibori, E.; Takata, M.; Sakata, M.; Shinohara, H. C_{66} fullerene encaging a scandium dimer. *Nature* **2000**, *408*, 426.

(10) Olmstead, M. M.; Lee, H. M.; Duchamp, J. C.; Stevenson, S.; Marciu, D.; Dorn, H. C.; Balch, A. L. $Sc_3N@C_{68}$: Folded Pentalene Coordination in an Endohedral Fullerene that Does Not Obey the Isolated Pentagon Rule. *Angew. Chem. Int. Ed.* **2003**, *42*, 900-903.

(11) Cai, T.; Xu, L.; Shu, C.; Reid, J. E.; Gibson, H. W.; Dorn, H. C. Synthesis and Characterization of a Non-IPR Fullerene Derivative: $Sc_3N@C_{68}[C(COOC_2H_5)_2]$. *J. Phys. Chem. C* **2008**, *112*, 19203-19208.

(12) Amsharov, K. Y.; Ziegler, K.; Mueller, A.; Jansen, M. Capturing the Antiaromatic $^{\#6094}C_{68}$ Carbon Cage in the Radio-Frequency Furnace. *Chem. Eur. J.* **2012**, *18*, 9289-9293.

(13) Dang, J.-S.; Zheng, J.-J.; Wang, W.-W.; Zhao, X. Open-Shell Triplet Character of $^{\#6094}C_{68}$: Spherical Aromaticity, Thermodynamic Stability, and Regioselective Chlorination. *Inorg. Chem.* **2013**, *52*, 4762-4764.

(14) Jin, P.; Li, Y.; Magagula, S.; Chen, Z. Exohedral functionalization of endohedral metallofullerenes: Interplay between inside and outside. *Coord. Chem. Rev.* **2019**, *388*, 406-439.

(15) Osuna, S.; Swart, M.; Solà, M. The reactivity of endohedral fullerenes. What can be learnt from computational studies? *Phys. Chem. Chem. Phys.* **2011**, *13*, 3585-3603.

(16) Hirsch, A. *The Chemistry of Fullerenes*; Thieme: Sttutgart, Germany, 1994.

(17) Garcia-Borràs, M.; Osuna, S.; Swart, M.; Luis, J. M.; Solà, M. Electrochemical control of the regioselectivity in the exohedral functionalization of C_{60}: the role of aromaticity. *Chem. Commun.* **2013**, *49*, 1220-1222.

(18) El Bakouri, O.; Garcia-Borràs, M.; Girón, R. M.; Filippone, S.; Martín, N.; Solà, M. On the regioselectivity of the Diels–Alder cycloaddition to C_{60} in high spin states. *Phys. Chem. Chem. Phys.* **2018**, *20*, 11577-11585.

(19) Yang, T.; Zhao, X.; Nagase, S.; Akasaka, T. Diels–Alder Reaction on Free C_{68} Fullerene and Endohedral $Sc_3N@C_{68}$ Fullerene Violating the Isolated Pentagon Rule: Importance of Pentagon Adjacency. *Chem. Asian J.* **2014**, *9*, 2604-2611.

(20) Frisch, M. J.; Trucks, G. W.; Schlegel, H. B.; Scuseria, G. E.; Robb, M. A.; Cheeseman, J. R.; Scalmani, G.; Barone, V.; Petersson, G. A.; Nakatsuji, H.; Li, X.; Caricato, M.; Marenich, A. V.; Bloino, J.; Janesko, B. G.; Gomperts, R.; Mennucci, B.; Hratchian, H. P.; Ortiz, J. V.; Izmaylov, A. F.; Sonnenberg, J. L.; Williams; Ding, F.; Lipparini, F.; Egidi, F.; Goings, J.; Peng, B.; Petrone, A.; Henderson, T.; Ranasinghe, D.; Zakrzewski, V. G.; Gao, J.; Rega, N.; Zheng, G.; Liang, W.; Hada, M.; Ehara, M.; Toyota, K.; Fukuda, R.; Hasegawa, J.; Ishida, M.; Nakajima, T.; Honda, Y.; Kitao, O.; Nakai, H.; Vreven, T.; Throssell, K.; Montgomery Jr., J. A.; Peralta, J. E.; Ogliaro, F.; Bearpark, M. J.; Heyd, J. J.; Brothers, E. N.; Kudin, K. N.; Staroverov, V. N.; Keith, T. A.; Kobayashi, R.; Normand, J.; Raghavachari, K.; Rendell, A. P.; Burant, J. C.; Iyengar, S. S.; Tomasi, J.; Cossi, M.; Millam, J. M.; Klene, M.; Adamo, C.; Cammi, R.; Ochterski, J. W.; Martin, R. L.; Morokuma, K.; Farkas, O.; Foresman, J. B.; Fox, D. J.; Gaussian 16 Rev. B.01: Wallingford, CT, 2016.

(21) Becke, A. D. Density-functional thermochemistry. III. The role of exact exchange. *J. Chem. Phys.* **1993**, *98*, 5648-5652.

(22) Lee, C.; Yang, W.; Parr, R. G. Development of the Colle-Salvetti correlation-energy formula into a functional of the electron density. *Phys. Rev. B* **1988**, *37*, 785-789.

(23) Grimme, S.; Antony, J.; Ehrlich, S.; Krieg, H. A consistent and accurate ab initio parametrization of density functional dispersion correction (DFT-D) for the 94 elements H-Pu. *J. Chem. Phys.* **2010**, *132*, 154104.

(24) Frisch, M. J.; Pople, J. A.; Binkley, J. S. Self-consistent molecular orbital methods 25. Supplementary functions for Gaussian basis sets. *J. Chem. Phys.* **1984**, *80*, 3265-3269.

(25) Bickelhaupt, F. M.; Baerends, E. J. In *Rev. Comput. Chem.*; Lipkowitz, K. B., Boyd, D. B., Eds.; Wiley-VCH: New York, 2000; Vol. 15, p 1-86.

(26) Fernández, I.; Bickelhaupt, F. M. The activation strain model and molecular orbital theory: understanding and designing chemical reactions. *Chem. Soc. Rev.* **2014**, *43*, 4953-4967.

(27) Bickelhaupt, F. M.; Houk, K. N. Analyzing Reaction Rates with the Distortion/Interaction-Activation Strain Model. *Angew. Chem. Int. Ed.* **2017**, *129*, 10070-10086.

(28) Wolters, L. P.; Bickelhaupt, F. M. The activation strain model and molecular orbital theory. *WIREs Comput. Mol. Sci.* **2015**, *5*, 324-343.

(29) Fernández, I. Understanding the Reactivity of Fullerenes Through the Activation Strain Model. *Eur. J. Org. Chem.* **2018**, *2018*, 1394-1402.

(30) Weigend, F.; Ahlrichs, R. Balanced basis sets of split valence, triple zeta valence and quadruple zeta valence quality for H to Rn: Design and assessment of accuracy. *Phys. Chem. Chem. Phys.* **2005**, *7*, 3297-3305.

(31) Kitaura, K.; Morokuma, K. A New Energy Decomposition Scheme for Molecular Interactions within the Hartree-Fock Approximation. *Int. J. Quantum Chem.* **1976**, *10*, 325-340.

(32) Morokuma, K. Why do molecules interact? The origin of electron donor-acceptor complexes, hydrogen bonding and proton affinity. *Acc. Chem. Res.* **1977**, *10*, 294-300.

(33) Ziegler, T.; Rauk, A. On the calculation of Bonding Energies by the Hartree-Fock-Slater Method. *Theor. Chim. Acta* **1977**, *46*, 1-10.

(34) Hopffgarten, M. v.; Frenking, G. Energy decomposition analysis. *WIREs Comput. Mol. Sci.* **2012**, *2*, 43-62.

(35) Mitoraj, M. P.; Michalak, A.; Ziegler, T. A Combined Charge and Energy Decomposition Scheme for Bond Analysis. *J. Chem. Theory Comput.* **2009**, *5*, 962-975.

(36) te Velde, G.; Bickelhaupt, F. M.; Baerends, E. J.; Fonseca Guerra, C.; van Gisbergen, S. J. A.; Snijders, J. G.; Ziegler, T. Chemistry with ADF. *J. Comput. Chem.* **2001**, *22*, 931-967.

(37) Neese, F.; Wennmohs, F.; Hansen, A. Efficient and accurate local approximations to coupled-electron pair approaches: An attempt to revive the pair natural orbital method. *J. Chem. Phys.* **2009**, *130*, 114108.

(38) Neese, F. The ORCA program system. *WIREs Comput. Mol. Sci.* **2012**, *2*, 73-78.

(39) Lee, T. J.; Taylor, P. R. A diagnostic for determining the quality of single-reference electron correlation methods. *Int. J. Quant. Chem.* **1989**, *36*, 199-207.

(40) Garcia-Borràs, M.; Romero-Rivera, A.; Osuna, S.; Luis, J. M.; Swart, M.; Solà, M. The Frozen Cage Model: A Computationally Low-Cost Tool for Predicting the Exohedral Regioselectivity of Cycloaddition Reactions Involving Endohedral Metallofullerenes. *J. Chem. Theory Comput.* **2012**, *8*, 1671-1683.

(41) Fernández, I.; Solà, M.; Bickelhaupt, F. M. Origin of Reactivity Trends of Noble Gas Endohedral Fullerenes $Ng_2@C_{60}$ (Ng = He to Xe). *J. Chem. Theory Comput.* **2014**, *10*, 3863-3870.

(42) García-Rodeja, Y.; Solà, M.; Bickelhaupt , F. M.; Fernández, I. Reactivity and Selectivity of Bowl-Shaped Polycyclic Aromatic Hydrocarbons: Relationship to C_{60}. *Chem. Eur. J.* **2016**, *22*, 1368-1378.

(43) García-Rodeja, Y.; Solà, M.; Fernández, I. Understanding the Reactivity of Planar Polycyclic Aromatic Hydrocarbons: Towards the Graphene Limit. *Chem. Eur. J.* **2016**, *22*, 10572-10580.

(44) García-Rodeja, Y.; Solà, M.; Bickelhaupt, F. M.; Fernández, I. Understanding the Reactivity of Ion-Encapsulated Fullerenes. *Chem. Eur. J.* **2017**, *23*, 11030-11036.

(45) Fernández, I.; Solà, M.; Bickelhaupt, F. M. Why Do Cycloaddition Reactions Involving C_{60} Prefer [6,6] over [5,6] Bonds? *Chem. Eur. J.* **2013**, *19*, 7416-7422.

(46) Garcia-Borràs, M.; Osuna, S.; Luis, J. M.; Swart, M.; Solà, M. A Complete Guide on the Influence of Metal Clusters in the Diels–Alder Regioselectivity of I_h-C_{80} Endohedral Metallofullerenes. *Chem. Eur. J.* **2013**, *19*, 14931-14940.

(47) Hung, R. R.; Grabowski, J. J. A precise determination of the triplet energy of carbon (C_{60}) by photoacoustic calorimetry. *J. Phys. Chem.* **1991**, *95*, 6073-6075.

(48) Haddon, R. C. POAV3 program. *QCPE 508/QCMP 044, QCPE Bull.* **1988**, 8.

(49) Haddon, R. C. Measure of nonplanarity in conjugated organic molecules: which structurally characterized molecule displays the highest degree of pyramidalization? *J. Am. Chem. Soc.* **1990**, *112*, 3385-3389.